Large-Scale and High-Density pMUT Array Based on Isolated Sol-Gel PZT Membranes for Fingerprint Imaging

Yuan-Quan Chen, Yu-Xing Li, Yan Chen, Zhen-Yi Ju, Lu-Qi Tao, Yu Pang, Yi Yang, and Tian-ling Ren[z]

Institute of Microelectronics and Tsinghua National Laboratory for Information Science and Technology (TNList), Tsinghua University, Beijing 100084, People's Republic of China

In this work, we proposed a novel ultrasonic transducer array based on an array of 50 × 50 piezoelectric micromachined ultrasonic transducers (pMUTs). The structure was specially designed for fingerprint imaging application. The pMUTs array were fabricated with isolated piezoelectric lead zirconate titanate (PZT) cells to reduce the crosstalk between adjacent units, and released by deep-silicon etching from the back side. The cell size and pitch of pMUTs were 50 μm and 100 μm, respectively. Layer-by-layer annealing method was used instead of one-time annealing during the fabrication of sol-gel based PZT film. The resonance frequency of the pMUT was about 24.82 MHz which agreed well with simulated 25.02 MHz. Besides, the effective electro-mechanical coupling coefficient (k_{eff}) and mechanical quality factor (Q factor) of the transducer were 0.1293 and 198, respectively. The equivalent circuit of the transducer was established and analyzed. The fitted admittance circle agreed well with the experimental result. This demonstration of pMUTs array has profound potential for large-scale, high-density, and high-frequency fingerprint imaging.
 [DOI: 10.1149/2.0891707jes]

Manuscript submitted March 15, 2017; revised manuscript received May 1, 2017. Published May 17, 2017.

Optical, capacitive, piezoelectric and acoustic mechanisms based sensors have been developed to capture the electronic images of human fingerprints in the last twenty years.[1] The capacitive fingerprint sensors are the most widely used in consumer electronics, duo to their high array density and complementary metal-oxide-semiconductor transistor (CMOS) compatibility.[2–4] However, the image captured by capacitive fingerprint sensor is two-dimensional, which can be spoofed easily by a printed template. And capacitive fingerprint sensors are extremely sensitive to contamination and moisture on the finger, which may lead to false recognition. Ultrasonic transducer array provides a potential solution to these problems. The acoustic impedances of valleys and ridges on fingerprints are greatly different, and can be easily distinguished by ultrasonic transducer.[5] Thus, the ultrasonic pulse-echo imaging technology can be applied to imaging the ridges, valleys of the fingerprints, and even the tissue beneath. The three-dimensional images captured by ultrasonic fingerprint sensor eliminates the risks of failure and spoof.[6] Large-scale, high-density pMUTs array based on AlN were used in high resolution fingerprint imaging with small size, high frame-rate and low cost.[7,8] The lead zirconate titanate (PZT) has piezoelectric coefficient that is generally two-orders-of-magnitude higher than AlN,[9–11] which can be used to fabricate fingerprint sensor with better performance. A PZT based fingerprint sensor was reported with single-pixel and mechanical-scanning working mode, which was large size, low frame-rate, and high cost.[12]

In this report, we demonstrate an ultrasound transducers array for fingerprint imaging based on sol-gel PZT technique. We designed the structures and parameters of the transducer by simulation, and fabricated the arrays of pMUTs based on the sol-gel PZT techniques.[13] The isolated piezoelectric membranes were used to reduce the crosstalk between adjacent units. The cell size and pitch of pMUTs were 50 μm and 100 μm, respectively, which could meet the resolution demand of the fingerprint identification. Based on simulation and design, we fabricated and characterized the pMUTs array with good performances. The resonance frequency of the pMUT was about 24.82 MHz which agreed well with the simulated 25.02 MHz. The effective electro-mechanical coupling coefficient (k_{eff}) and mechanical quality factor transducer (Q factor) were 0.1293 and 198, respectively. The equivalent circuit of the transducer was analyzed and established. The fitted admittance circle agreed well with the experimental result.

[z]E-mail: RenTL@tsinghua.edu.cn

Transducer Geometry Design and Simulation

The schematic cross-section view of the pMUTs with designed Al/Pt/PZT/Pt/TiO_2/SiO_2/Si structure is shown in Fig. 1. The SiO_2 and Si were used as insulating layer and mechanically supporting substrate, respectively. The PZT layer was chosen because of its high piezoelectric coefficient. The Pt layers worked as the electrodes and barriers to prevent the diffusion of PZT. The TiO_2 layer served as the adhesion layer between Pt and SiO_2. The top Al layer was used as wiring and bonding pads. Fig. 2 shows the 3D model of a small 4 × 4 array as demonstration. The real device is 50 × 50 array with high density. Due to the large quantity of pMUT units (2500 units), it was impossible to wiring every unit separately. So the row and column addressing lines were used to solve this problem. This method has been proved to be a feasible method for control and imaging.[14–16]

The vibration mode and resonant frequency of the designed device were analyzed in advance. The resonance frequency of the pMUT device is essential, because it is the determining factor for resolution and depth of penetration. Thus, the proper structural design for controlling the resonance frequency is of great significance. In this work, the finite elements analysis (FEA) of a single pMUT was carried out by using COMSOL Multiphysics. As the COMSL model shown in Fig. 3, only a quarter of the symmetric structure was drawn for the simulation to speed up simulation efficiency. As show in Fig. 3a, the vibration mode at 25.02 MHz was the basic mode of the membrane-bending vibration which had the highest displacement and the best emitting performance. The charge density in response to an uniform sound pressure was analyzed as presented in Fig. 3b. The induced charges were positive at the central area of the PZT membrane. However, they turned negative at the edges. The border located at around 70% of the membrane length. So, in order to achieve better reception sensitivity, the area of the top Pt electrode was design to be smaller than whole PZT membrane.[17] The designed physical parameters of the pMUTs are summarized in Table I. The simulated resonance frequency was 25.02 MHz meeting the requirement for fingerprint imaging.

Fabrication

Based on the simulation and design, we fabricated the devices by following the process described in Fig. 4. The 200 μm Si wafer was used instead of 500 μm wafer in order to reduce the difficulty of back side deep-silicon etching and improve the etching accuracy. The 200 nm thermal oxide layer was grown as insulating layer. The 30 nm Ti layer was sputtered for forming an adhesive layer for Pt electrodes. Then, the Ti layer was oxidized to TiO_2 by using

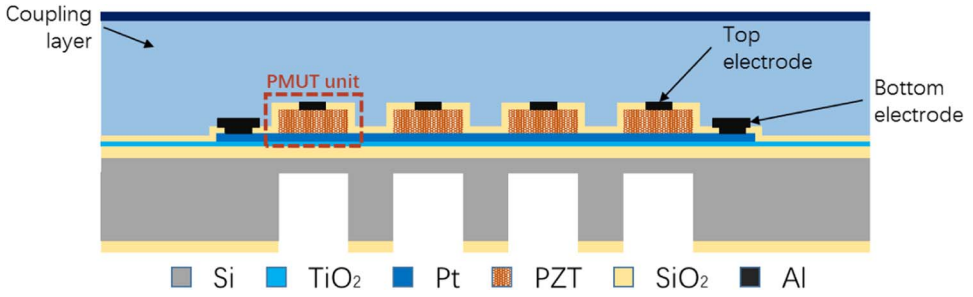

Figure 1. Cross-section diagram of the device.

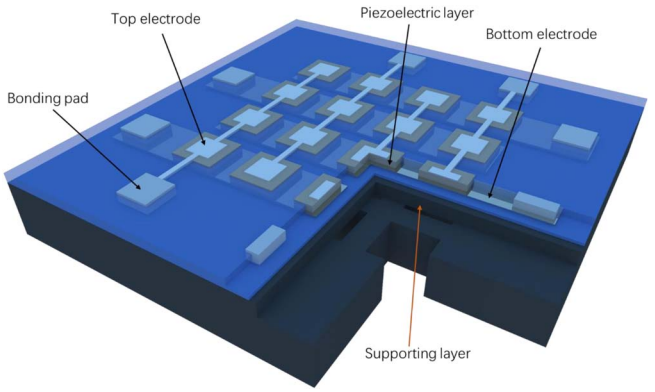

Figure 2. 3D schematic of the device.

Table I. Structural parameters of the pMUT.

Parameter	Value
Thickness of Si	10 μm
Thickness of SiO_2	0.2 μm
Thickness of bottom Pt	0.2 μm
Thickness of PZT	1 μm
Thickness of top Pt	0.2 μm
Area of PZT	50 μm × 50 μm
Area of top Pt	30 μm × 30 μm

high-temperature oxidation furnace before sputtering of Pt. The reason for this step was that the oxidation of Ti during the subsequent high-temperature PZT crystallization might result in the damage of the upper Pt layer and failure of the device. The 200 nm Pt was patterned and deposited as the bottom electrode and barrier layer to prevent the diffusion of PZT. The 1 μm piezoelectric PZT layer was deposited by sol-gel techniques and patterned by wet etching. The etching solution was a mixture of 60 mL 36 wt% HCl, 1 mL 40 wt% HF, and 140 mL deionized water. The etched PZT cells were 50 μm × 50 μm isolated membranes with 100 μm pitches. Subsequently, bottom Pt electrodes were patterned by lithography and reactive ion etching (RIE). The 200 nm SiO_2 insulating layer was deposited by plasma enhanced chemical vapor deposition (PECVD) and patterned by RIE. The 200 nm Pt top electrodes were fabricated by sputtering and lift off. The 600 nm Al pads covering the Pt top electrodes were deposited for wire bonding. The structure was released by using deep-silicon etching with precisely controlled etching rate of 1 μm per minute. During this step, etching time was deliberately controlled so that 10 μm silicon layer was remained as mechanically supporting layer.

The PZT film was spin coated on the substrate layer by layer for 10 times. The thickness of the PZT film was 1 μm in total. For each layer, the hot baking and pyrolysis processes were carried out under 250°C for 2 mins and under 350°C for 5 mins, respectively. High-temperature annealing was of great importance for the crystallization of the PZT films. In order to obtain PZT films with good performance, each spin-coated PZT layer was separately subjected to the high-temperature crystallization after the spin-coating, hot-baking and pyrolysis processes. This method was much better than the one-time annealing method after the deposition of the whole 1 μm PZT film. In this way,

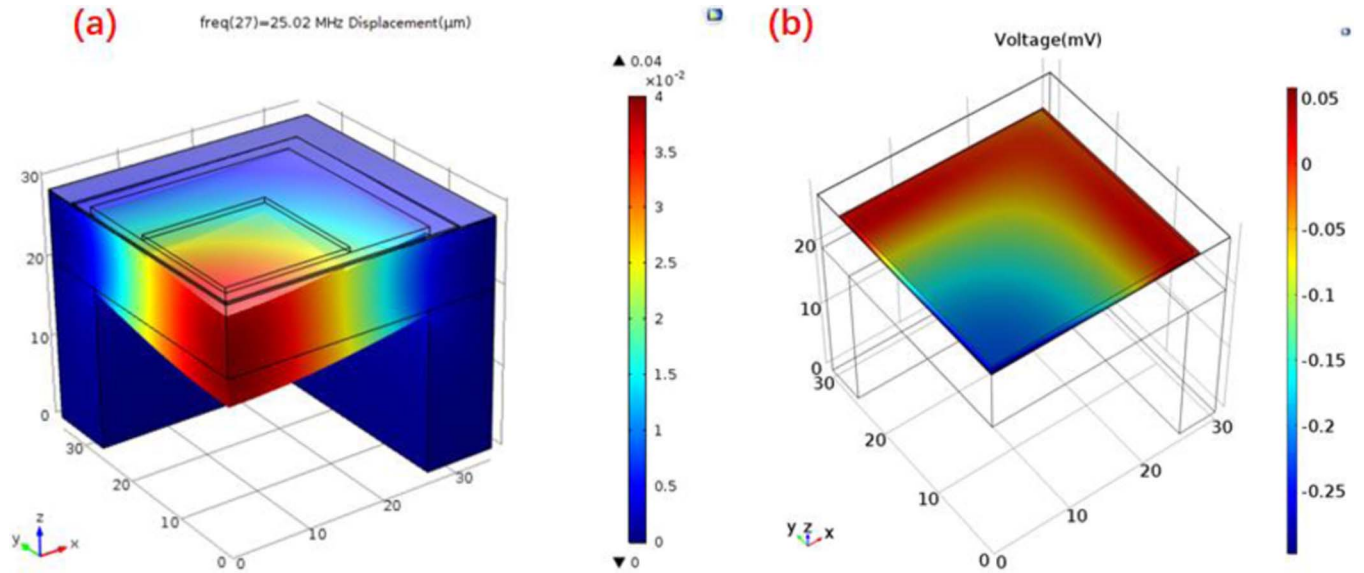

Figure 3. (a) The displacement of the membrane at the resonance frequency; (b) The charge density on the membrane in response to an uniform sound pressure.

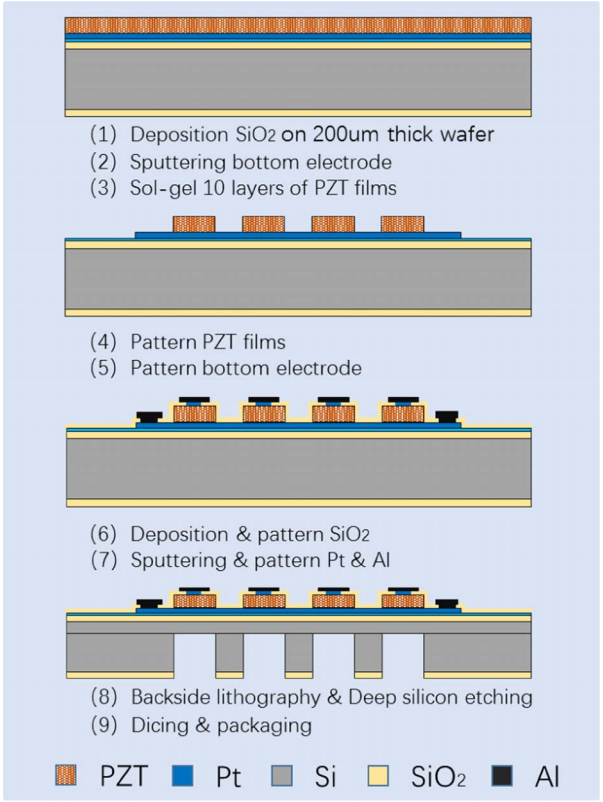

Figure 4. Fabrication process of the device.

the residual stress of each PZT layer was released, so that the crack of the 1 μm PZT film was avoided. Besides, because the upper PZT layers were grown and crystallized based on the first spin-coated layer, the crystal state of the first layer had a great influence on the quality of

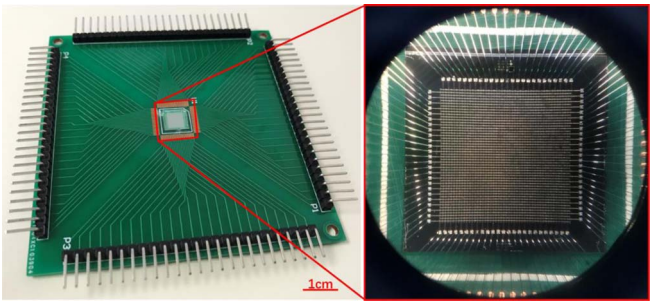

Figure 6. Photo of the packaged pMUTs chip.

the whole PZT film. Thus, the annealing time of the first spin-coated PZT layer was extended to 20 mins for reinforcing the crystallization.

Figs. 5a and 5b present a cross-section image of the PZT film and a SEM image of isolated PZT membrane, respectively. The roughness of the etched PZT edges was less than 1 μm which was much smaller than the size of the isolated PZT membranes, so its influence was negligible. Fig. 5c shows the array of the fabricated pMUTs. Each pMUT was a piezoelectric membrane with a 10 μm Si elastic layer, 200 nm Pt bottom electrode, 1 μm PZT piezoelectric layer, and 200 nm Pt top electrode covered with 600 nm Al as pad.

After dicing, assembly, and wire bonding, the testable device was completed. After packaging, the device was ready for polarizing to achieve piezoelectric property. Before polarizing, the chip was stuck on a print circuit board (PCB) with silica gel which could remain steady under 200°C, as shown in Fig. 6. The chip was first heated to 180°C. Then a 18 V DC voltage was applied on the PZT membranes for 10 minutes. Then, the voltage was maintained after the heated was closed until that the sample was naturally cooled to the room temperature.

Characterization

The impedance-frequency spectrum of the micromachined ultrasonic transducer measured by HP 4294A impedance phase analyzer is

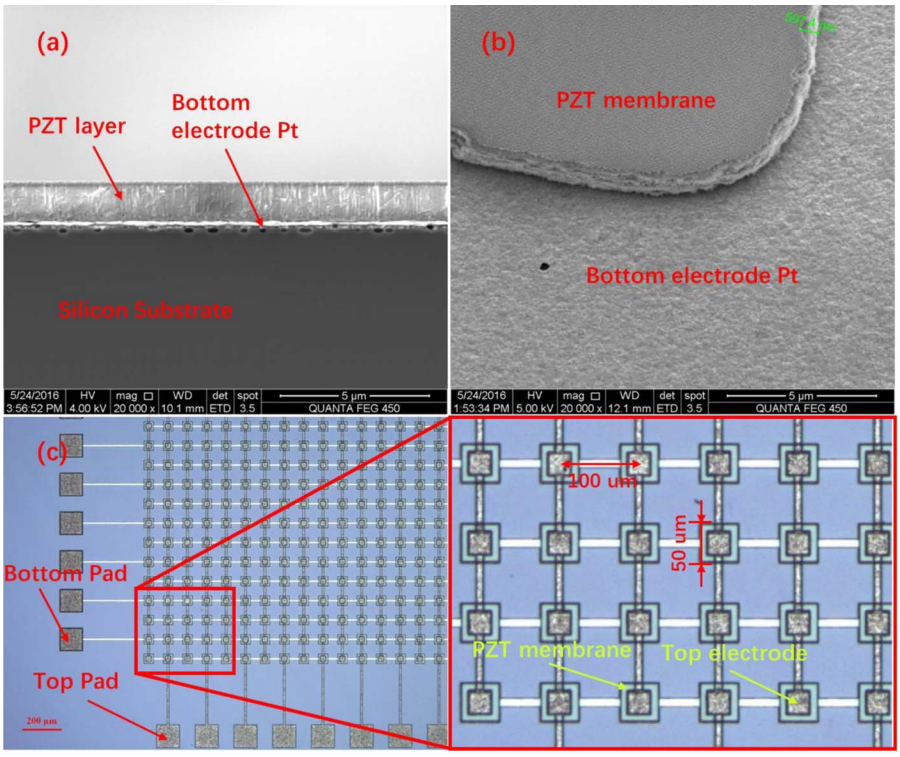

Figure 5. (a) Cross-section SEM image of PZT film. (b) SEM image of isolated PZT membrane with bottom electrode. (c) Optical images of the 50 × 50 PMUT array.

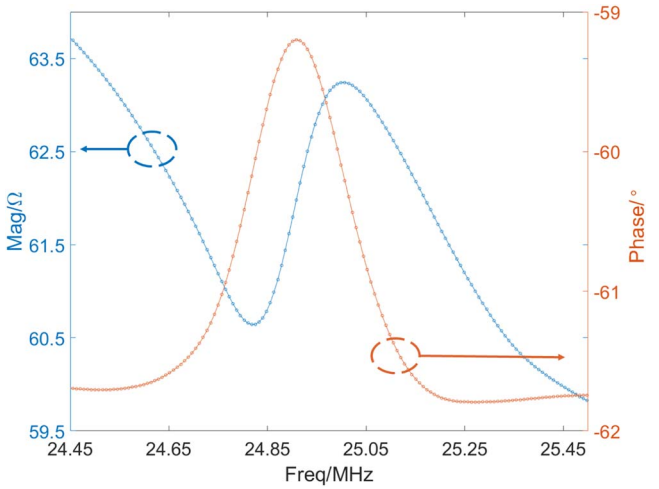

Figure 7. The impedance-frequency spectrum of the pMUT.

shown in Fig. 7. The resonance frequency derived from the impedance-frequency spectrum was 24.82 MHz. This experimental result agreed well with simulated 25.02 MHz mentioned above. The difference between them may be resulted by the residue stress in the structure. The effective electro-mechanical coupling coefficient (k_{eff}) was defined in IEEE Std 176–1987 for evaluating the electromechanical coupling regardless of the geometry and excitation style of the piezoelectric resonator.[18] It is defined as the equation below:

$$k_{eff}^2 = 1 - (f_r/f_a)^2 \quad [1]$$

where f_r and f_a are the resonance frequency and anti-resonance frequency, respectively. The k_{eff} of the pMUT transducer was 0.1293, which was calculated according to its impedance-frequency spectrum using Eq. 1.

The equivalent circuit of the transducer near the resonance frequency was established as shown in Fig. 8a, where C_0, L_1, C_1, R_1, and R_n are static capacitance, inductor, capacitance, resistance of the dynamic impedance, and loss resistance of the transducer, respectively. Besides, the R_0 was used to indicate the series resistance induced by the connection, because there were relatively long wires between the device and the test equipment.

Table II. The parameters of the equivalent circuit.

Parameter	$C_0(pF)$	$L_1(H)$	$C_1(fF)$	$R_1(\Omega)$	$R_n(\Omega)$	$R_0(\Omega)$
Value	91.16	2.1E-03	19.41	1.66E + 03	127.46	15

Generally, the admittance Y of a network is:

$$Y = G + jB \quad [2]$$

where G and B are the real and imaginary parts of Y which stand for the conductance and susceptance, respectively. For our transducer, the conductance and susceptance under certain angular frequencies can be got from the impedance-frequency spectrum. So, the experimental admittance circle shown in Fig. 8b was deduced from the impedance-frequency spectrum presented in Fig. 7. For the equivalent circuit of our transducer, the admittance Y_t is:

$$Y_t = G_t + jB_t = \frac{Y_0}{1 + R_0 Y_0} \quad [3]$$

$$Y_0 = j\omega C_0 + \frac{1}{R_n} + \frac{1}{R_1 + j\left(\omega L_1 - \frac{1}{\omega C_1}\right)} \quad [4]$$

where ω and Y_0 are the angular frequency and the admittance of the transducer itself. Based on the experimental admittance circle, the parameters of the equivalent circuit were calculated and fitted by using numerical methods (Matlab). The results are listed in Table II. As shown in Fig. 8b, the fitted admittance circle agreed well with the experimental data. The deviation between them might be caused by the parasitic inductances introduced by the connections.

Based on the obtained equivalent circuit, the Q factor of the transducer can be calculated according to the following equation:

$$Q = \frac{1}{R_1}\sqrt{\frac{L_1}{C_1}} \quad [5]$$

where the R_1, C_1, and L_1 are the corresponding parameters in the equivalent circuit. The calculated Q factor of the fabricated pMUT transducer was about 198, which was higher than the Q factor of 111 in Ref. 4. Thus, our pMUT transducer presented much better launching performance than the previous work.

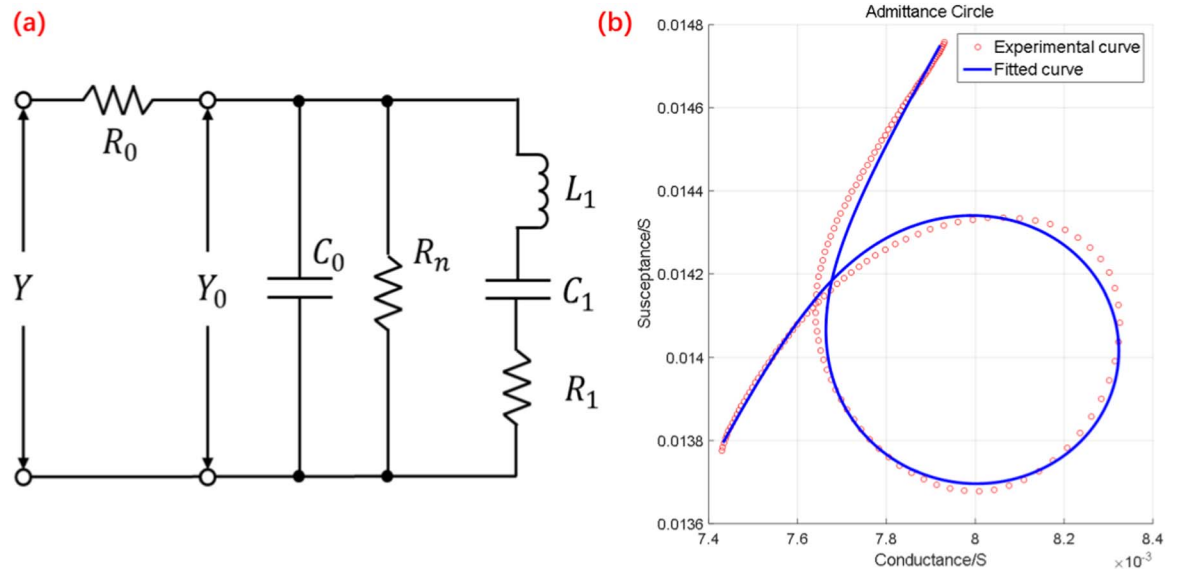

Figure 8. (a) The equivalent circuit of the transducer. (b) The experimental data and fitted result of the admittance circles.

Conclusions

In conclusion, an ultrasound-transducer array for fingerprint imaging based on sol-gel PZT technique was demonstrated. The structure of pMUT was simulated by using FEA method. The resonance frequency of the pMUTs was designed to be around 25.02 MHz. The pMUTs array were fabricated with isolated piezoelectric cells to reduce the crosstalk between adjacent units. The structure was released by deep-silicon etching from the back side. The size and pitch of pMUTs were 50 μm and 100 μm, respectively, which met the resolution demand of fingerprint imaging. The details and optimizations of the fabrication process were described. The measured resonance frequency of the pMUTs was about 24.82 MHz which agreed well with the design. The k_{eff} and Q factor of the transducer were 0.1293 and 198, respectively. The equivalent circuit of the transducer was established and analyzed. The fitted admittance circle agreed well with the experimental data. This device was specially designed for fingerprint imaging and presented with excellent performances. The designed row and column addressing lines allowed the wire bonding between the ultrasonic transducer array and integrated circuitry, which can form practical ultrasonic fingerprint sensors. Our demonstration of sol-gel PZT based pMUTs array is remarkably promising for large-scale, high-density, and high-frequency fingerprint imaging application.

Acknowledgments

This work was supported by the National Natural Science Foundation (61574083, 61434001), National Basic Research Program (2015CB352101), National Key Research and Development Program (2016YFA0200400), National Key Project of Science and Technology (2011ZX02403-002), and Special Fund for Agroscientific Research in the Public Interest (201303107) of China. The authors are also thankful for the support of the Independent Research Program (2014Z01006) of Tsinghua University, and Advanced Sensor and Integrated System Lab of Tsinghua University Graduate School at Shenzhen (ZDSYS20140509172959969).

References

1. S. Memon, M. Sepasian, and W Balachandran, Review of finger print sensing technologies. In *Multitopic Conference, 2008. INMIC 2008. IEEE International* (pp. 226). IEEE (2008, December).
2. J. W. Lee, D. J. Min, J. Kim, and W. A Kim, 600-dpi capacitive fingerprint sensor chip and image-synthesis technique. *IEEE Journal of Solid-State Circuits*, **34**(4), 469 (1999).
3. J. M. Nam, S. M. Jung, and M. K. Lee, Design and implementation of a capacitive fingerprint sensor circuit in CMOS technology. *Sensors and Actuators A: Physical*, **135**(1), 283 (2007).
4. H. Morimura, S. Shigematsu, and K. Machida, A novel sensor cell architecture and sensing circuit scheme for capacitive fingerprint sensors. *IEEE Journal of Solid-State Circuits*, **35**(5), 724 (2000).
5. Y. Lu, H. Tang, S. Fung, Q. Wang, J. M. Tsai, M. Daneman, and D. A. Horsley, Ultrasonic fingerprint sensor using a piezoelectric micromachined ultrasonic transducer array integrated with complementary metal oxide semiconductor electronics. *Applied Physics Letters*, **106**(26), 263503 (2015).
6. X. Jiang, H. Y. Tang, Y. Lu, X. Li, J. M. Tsai, E. J. Ng, and D. A. Horsley, Monolithic 591× 438 DPI ultrasonic fingerprint sensor. In Micro Electro Mechanical Systems (MEMS), *2016 IEEE 29th International Conference on* (pp. 107). IEEE (2016, January).
7. H. Tang, Y. Lu, S. Fung, J. M. Tsai, M. Daneman, D. A. Horsley, and B. E. Boser, Pulse-echo ultrasonic fingerprint sensor on a chip. In Solid-State Sensors, Actuators and Microsystems (TRANSDUCERS), *2015 Transducers-2015 18th International Conference on* (pp. 674). IEEE (2015, June).
8. Y. Lu, D. Horsley, H. Y. Tang, and B. U. S. Boser, Pat. Application No. 14/896,150 (2014).
9. M. A. Dubois and P. Muralt, Measurement of the effective transverse piezoelectric coefficient e 31, f of AlN and Pb (Zr x, Ti 1−x) O 3 thin films. *Sensors and Actuators A: Physical*, **77**(2), 106 (1999).
10. P Muralt, PZT thin films for microsensors and actuators: Where do we stand?. *IEEE transactions on ultrasonics, ferroelectrics, and frequency control*, **47**(4), 903 (2000).
11. S. Trolier-McKinstry and P. Muralt, Thin film piezoelectrics for MEMS. *Journal of Electroceramics*, **12**(1), 7 (2004).
12. J. K. Schneider and S. M. Gojevic, Ultrasonic imaging systems for personal identification. In *Ultrasonics Symposium*, 2001 IEEE (Vol. **1**, pp. 595). IEEE (2001).
13. K. Budd, S. K. Dey, and D. A. Payne, SOL-GEL PROCESSING OF PbTiO//3, PbZrO//3, PZT, AND PLZT THIN FILMS. In *British Ceramic Proceedings. Inst of Ceramics* (1985).
14. M. F. Rasmussen and J. A. Jensen, 3-D ultrasound imaging performance of a row-column addressed 2-D array transducer: A measurement study. In *Ultrasonics Symposium (IUS)*, 2013 IEEE International (pp. 1460). IEEE (2013, July).
15. L. L. Wong, A. I. Chen, Z. Li, A. S. Logan, and J. T Yeow, A row–column addressed micromachined ultrasonic transducer array for surface scanning applications. *Ultrasonics*, **54**(8), 2072 (2014).
16. A. S. Logan, L. L. Wong, A. I. Chen, and J. T. Yeow, A 32 x 32 element row-column addressed capacitive micromachined ultrasonic transducer. *IEEE transactions on ultrasonics, ferroelectrics, and frequency control*, **58**(6), 1266 (2011).
17. D. Fu, T. L. Ren, H. Chen, Y. Yang, X. M. Kong, Y. Ren, and L. T. Liu, A novel method for fabricating 2-D array piezoelectric micromachined ultrasonic transducers for medical imaging. In *Applications of Ferroelectrics, 2009. ISAF 2009*. 18th IEEE International Symposium on the(pp. 1). IEEE (2009, August).
18. T. R. Meeker, Publication and Proposed Revision of ANSI/IEEE Standard 176-1987. *IEEE Transactions on Ultrasonics Ferroelectrics and Frequency Control*, **43**(5), 717 (1996).